# Anisotropic model building from logs in vertical wells

*Yunyue Elita Li, Arthur Cheng, and Aaron Fong*
*Department of Civil and Environmental Engineering, National University of Singapore*

## SUMMARY

Anisotropic parameters are widely needed in seismic imaging and reservoir characterization in modern seismic exploration industry. Unlike other elastic parameters such as P- and S-wave velocities, anisotropic parameters are not measured directly from the well logs due to the single directional nature of a well. We propose to estimate anisotropy parameters from the vertical well logs based on the Hudson-Cheng's model for anisotropy. We assume that anisotropy is induced by inclusions of weak cracks that are filled with water in a background isotropic medium, whose bulk and shear moduli are inverted from the vertical measured P- and S-wave velocities (vertical pressure and shear modulus). In this abstract, we discuss the method of the anisotropic model building and compare the anisotropy parameters estimated by the proposed method with that estimated by Stoneley wave inversion. Comparison with an offset well shows that the estimated anisotropy using the proposed method agrees with the mineralogy, whereas the Stoneley wave measurements are less than satisfactory at this well.

## INTRODUCTION

The importance of elastic anisotropy has increased dramatically as seismic acquisition demands longer offsets, wider azimuths, and multiple components. Inaccuracy of elastic anisotropy may lead to poor seismic images, large depth errors, and misinterpretation of the lithology. However, anisotropy model building is an extremely challenging task due to the limited data we afford to acquire in the field. Although seismic data cover large area, accuracy of the velocity and anisotropy models derived from the seismic data inversion is usually too low for direct lithological interpretation. Well log measurements at sparse well locations, on the other hand, have been used to calibrate the seismic data and to initialize the lithological inversion based on the amplitude-versus-angle measurements. Nonetheless, direct measurements of anisotropy are not available in routine downhole measurements.

Among the commonly available well logging measurements, gamma ray, density, and porosity measurements are measured as non-directional parameters. Due to the constraints on the trajectory of a well, downhole sonic measurements are usually single-directional, which leads to P- and S-wave slownesses measured in the vertical direction in most of the wells. Thus, we can easily determine the two elastic constants that are determined by the vertical propagating P- and S-waves: $C_{33} = \rho V_p^2$ and $C_{44} = \rho V_{sv}^2$. Recently, Stoneley wave measurements are proposed to be inverted to assess the anisotropy characteristics of a formation, due to their sensitivity to the SH wave at the low-frequency limit (Cheng et al., 1983; Tang, 2003). However, Stoneley waves measurements can be highly unstable due to slight borehole variations caused by invasion. Moreover, Stoneley waves' sensitivity to the SH wave reduces when the formation S-wave velocity is too fast compared with the borehole fluid P-wave velocity. To the best of our knowledge, we do not have direct P-wave anisotropy measurements from the well logs, which is strongly needed by seismic imaging and lithological inversion (Li et al., 2011; Yang et al., 2012; Li et al., 2016).

Many authors (Hornby et al., 1994; Sayers, 1995; Vernik and Liu, 1997; Bandyopadhyay, 2009; Bachrach, 2010) have built averaged depth trends based on well log and lab measurements in order to guide seismic processing. Due to the complexity of the rock physics model and the lack of measurement in the data, large uncertainty exist in the rock physics modeling exercises. Therefore, most of the rock physics exercises describe the qualitative depth trends of anisotropy, without providing quantitative information. Bachrach (2010) and Li et al. (2013) managed to utilize stochastic rock physics modeling schemes to capture the uncertainties in the modeling process, and demonstrated that the rock physics modeling results can be used to constrain seismic imaging and inversion. However, due to the somewhat arbitrary choices of the parameter uncertainties and their independency, the resulting rock physics models might not be fully consistent across different realizations of the input parameters.

In this paper, we propose to estimate formation anisotropy from vertical and non-direcional measurements assuming a crack rock physics model, which effectively characterizes the formation as a vertical transverse isotropic (VTI) medium. Retaining the first order perturbations to the background isotropic medium, we decompose the rock into three cascaded components: 1) a background homogenous isotropic rock matrix, which is fully determined by its mineral components, 2) a randomly distributed spherical pore space saturated with water, and 3) a set of aligned thin-cracks that accounts for the VTI anisotropy. To ensure a consistent rock physics model, we set up an inverse problem to estimate the parameters that are not directly measured by the well logs.

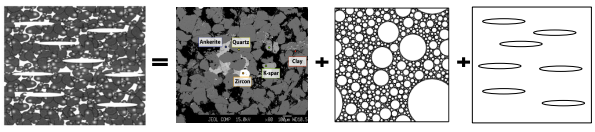


Figure 1: A Sketch of the decomposition of a complex rock sample to simple rock physics models: 1) a homogeneous isotropic rock matrix, 2) a set of randomly distributed spherical pores, and 3) a set of aligned thin-cracks.

We present the workflow using well log measurements provided by Halliburton. We compare the modeled anisotropy models with the mineral logs from a nearby well and demon-

strate that the modeled anisotropy agrees well with the lithology. We compare the modeled shear wave anisotropy using Hudson-Cheng's model with the "measured" shear wave anisotropy using Stoneley wave velocities, and confirmed that Stoneley waves measurements yield unstable estimations of shear wave anisotropy.

## HUDSON-CHENG'S ELLIPSOIDAL CRACK MODEL

Hudson (1981) and Cheng (1993) developed a second-order approximation for the effective moduli of a cracked medium by a scattering approach. We neglect the the second-order correction to the background moduli in the original formulation and utilize the first-order approximation in this paper. The effective elastic moduli are given by:

$$C_{ij}^{*} = C_{ij}^{0} + C_{ij}^{1}, \tag{1}$$

where the effective elastic moduli may be measured with downhole logging tools. $C_{ij}^{0}$ are the background moduli, which is assumed isotropic with circular inclusion of brine-saturated pores. $C_{ij}^{1}$ are the first-order correction. The background moduli are given by

$$\begin{aligned} C_{11}^{0} &= C_{33}^{0} = \lambda + 2\mu, \\ C_{13}^{0} &= \lambda, \\ C_{44}^{0} &= C_{66}^{0} = \mu, \end{aligned} \tag{2}$$

where $\lambda$ and $\mu$ are the Lame constants. The first-order corrections are given by

$$C_{11}^{1} = -\frac{\lambda^2}{\mu} d_c U_3, \tag{3}$$

$$C_{13}^{1} = -\frac{\lambda(\lambda+2\mu)}{\mu} d_c U_3, \tag{4}$$

$$C_{33}^{1} = -\frac{(\lambda+2\mu)^2}{\mu} d_c U_3, \tag{5}$$

$$C_{44}^{1} = -\mu d_c U_1, \tag{6}$$

$$C_{66}^{1} = 0, \tag{7}$$

where the crack density $d_c = \frac{3\phi_s}{4\pi\alpha}$ is defined by the ratio of the soft porosity $\phi_s$ and the aspect ratio $\alpha$ of the ellipsoidal cracks. For fluid-filled weak ($\alpha \ll 1$) inclusions,

$$\begin{aligned} U_3 &= \frac{4(\lambda+2\mu)}{3(\lambda+\mu)} \frac{1}{1+K}, \\ U_1 &= \frac{16(\lambda+2\mu)}{3(3\lambda+4\mu)}, \end{aligned} \tag{8}$$

with

$$K = \frac{K_f(\lambda+2\mu)}{\pi\alpha\mu(\lambda+\mu)}, \tag{9}$$

where $K_f$ is the bulk modulus of the fluid. In a vertical well, P-, S-wave velocity ($V_p$ and $V_s$) logs and density ($\rho$) logs provide measurement for the effective moduli of $C_{33}^{*}$ and $C_{44}^{*}$ where

$$\begin{aligned} C_{33}^{*} &= \rho V_p^2, \\ C_{44}^{*} &= \rho V_s^2. \end{aligned} \tag{10}$$

### Background moduli estimation by nonlinear parameter inversion

The background moduli can be estimated from the mineral components and the porosity if mineral logs are available. In most cases, however, mineral logs are less available than porosity and density logs in downhole measurements. In these cases, it is practical to assume the moduli of the background isotropic medium can be approximated by the Hashin-Shtrikman (HS) upper bound (Hashin and Shtrikman, 1962; Mavko et al., 2009), which is fully defined by the matrix moduli $(K_0, \mu_0)$, fluid moduli $(K_f, \mu_f)$, and the porosity $(\phi)$ as follows:

$$\begin{aligned} K^{HS+} &= K_0 + \frac{\phi}{(K_f - K_0)^{-1} + (1-\phi)(K_0 + \frac{4}{3}\mu_0)^{-1}}, \\ \mu^{HS+} &= \mu_0 + \frac{\phi}{(\mu_f - \mu_0)^{-1} + 2(1-\phi)\frac{K_0+2\mu_0}{5\mu_0(K_0+\frac{4}{3}\mu_0)}}. \end{aligned} \tag{11}$$

Further assuming $\lambda = K^{HS+} - \frac{2}{3}\mu^{HS+}$ and $\mu = \mu^{HS+}$, we can solve for the background matrix moduli $K_0, \mu_0$ and the aspect ratio $\alpha$ of the ellipsoidal cracks by solving the following nonlinear optimization problem:

$$J(K_0, \mu_0, \alpha) = \left\| \frac{\mu C_{33}^{1}}{(\lambda+2\mu)^2 U_3} - \frac{C_{44}^{1}}{\mu U_1} \right\|_2^2, \tag{12}$$

which ensures the crack density given by the P- and S-wave velocities are consistent with each other in Equation 5 and 6. Constrained by the P- and S-wave velocities, inversion for $K_0, \mu_0$ and $\alpha$ may show different sensitivities. Experiments show that the inversion has the best constraint on $\alpha$, and better constraint on $K_0$ compared with $\mu_0$. The multi-parameter distribution obtained by solving Equation 12 will help define the correlation of the parameters and reduce the search space when performing stochastic rock physics modeling for anisotropy.

With the solution of the optimization 12, we obtain the full stiffness tensor using Equations 3 to 7, and corresponding anisotropy parameters using Thomsen's definition.

$$\begin{aligned} \varepsilon &= \frac{C_{11} - C_{33}}{2C_{33}}, \\ \gamma &= \frac{C_{66} - C_{44}}{2C_{44}}, \\ \delta &= \frac{1}{2C_{33}^2}[2(C_{13}+C_{44})^2 - (C_{33}-C_{44})(C_{11}+C_{33}-2C_{44})]. \end{aligned} \tag{13}$$

These modeled anisotropy parameters are used as prior information when seismic data are inverted for anisotropy model building.

### Stonley wave measurement for shear wave velocity

A different way of estimating shear wave anisotropy $\gamma$ was described by Tang (2003) based on the Stoneley wave measurements. It has been shown that the tube wave velocity ($V_{ST}$) can be converted to the elastic modulus that determines the shear wave velocity with a horizontal polarization:

$$C_{66} = \frac{\rho_f V_f^2}{\frac{V_f^2}{V_{ST}^2} - 1}, \tag{14}$$

where $\rho_f$ and $V_f$ are the density and the P-wave velocity of the borehole fluid, $V_{ST}$ is the measured Stoneley wave speed at the low frequency limit. Stoneley wave speeds provide a direct measurement of the shear wave anisotropy when compared with the dipole shear wave velocities. However, it has been demonstrated that Stoneley wave may loose its sensitivity to shear wave velocity in fast formations, and is easily biased by the borehole or near borehole conditions.

## CASE STUDY

In this section we present the resulting anisotropy models based on the proposed workflow using well log data provided by Halliburton. Figure 2 shows the S-wave velocity by dipole and stoneley wave measurements, P-wave velocity, density, and porosity. Density log appears to be higher resolution than the rest of the log measurements because of different logging techniques. At depth around 1850 - 1870 ft, a sand layer can be identified from the high P- and S- velocities and low density. However, the neutron porosity measurement in the same layer is alarmingly low. Therefore, data conditioning is required to correct for the porosity measurements.

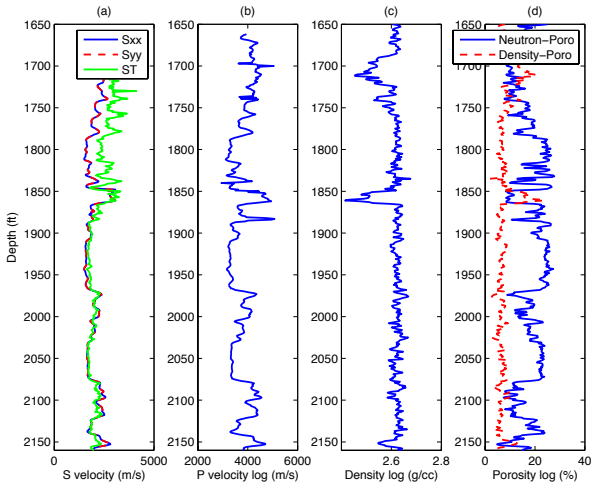


Figure 2: Halliburton well log data at a test well. Both dipole and Stoneley waves forms are inverted to get the shear wave velocity. P-wave velocity is derived from the monopole waveforms. Neutron-porosity logs show suspiciously large porosity values for shale formations due to the bounded water in illite. Therefore, we estimated the porosity using the density measurement instead.

Mineral logs in a nearby borehole show that the shale formations in this area are rich in illite, which may absorb significant amount of bounded water. Since the neutron tool infers porosity from the hydrogen content, it results in suspiciously large porosity measurements (up to 30%) in the shale formations. We determined subjectively that the porosity measurements are unrealistic and approximated the porosity from the density measurement instead. Estimated porosity from the density measurement is below 10%. Figure 2(d) shows the unreliable neutron porosity in blue and the density-porosity in red.

Assuming the rock is brine saturated with $K_f = 2.2$ GPa and $\mu_f = 0$, we solve the nonlinear optimization problem defined in 12 to estimate the matrix moduli $(K_0, \mu_0)$ and the aspect ratio $\alpha$ for two different lithological faces, shale and sand determined by a threshold of $\rho = 2.58$ g/cc. Figure 3 shows the histograms of $K_0, \mu_0$ and $\alpha$ within 95% confidence of the objective function. The histograms show that the inversion has much better constraints on $\alpha$ and $K_0$, than on $\mu_0$. Figure 3(d), which shows the objective function map at $\alpha = 0.0228$, suggested that many combinations of $K_0$ and $\mu_0$ could satisfy the objective function equally well, statistically speaking. Therefore, a subjective decision is required to define the best combination such that the resulting anisotropy is within a reasonable range. Alternatively, this multi-parameter distribution can be used for stochastic rock physics modeling (Li et al., 2013).

The subjectively selected background moduli and the aspect ratio for the two lithological facies are shown in Table 1. Figure 4(a) and (b) show the measured bulk and shear moduli scattered as a function of porosity in open circles. Measurements in the shale sections are highlighted in green. The red asterisks denote the estimated background moduli in the corresponding shale sections. Measurements in the sand sections are denoted in blue circles, and the black asterisks are the estimated background moduli in the sand sections. Figure 5(f) shows the estimated crack density, which shows great consistency with the micro-porosity log (light green in MRIL$^{TM}$ porosity) in a nearby offset well.

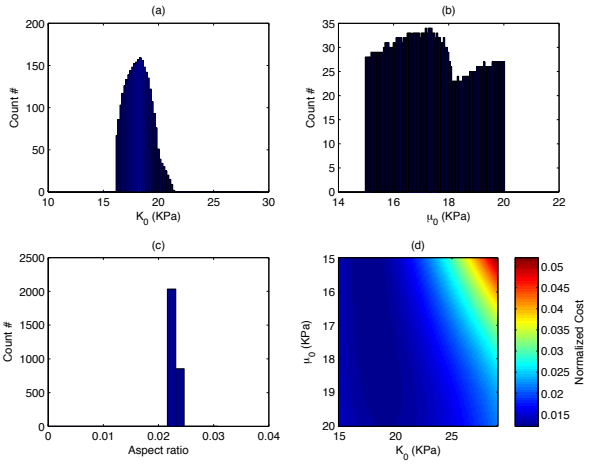


Figure 3: Histograms of $K_0$ in (a), $\mu_0$ in (b) and $\alpha_0$ in (c) within 95% confidence interval for the shale sections. In (d), a slice of the objective function is shown at $\alpha = 0.0228$. The flat valley suggests that many combinations of $K_0$ and $\mu_0$ satisfy the objective function 12 equally well.

| Facies | K (GPa) | $\mu$ (GPa) | $\alpha$ |
|---|---|---|---|
| Shale | 21.5772 | 15.5040 | 0.0228 |
| Sand | 29.5045 | 24.5041 | 0.0352 |

Table 1: Inverted parameters

Figure 5 shows the vertical velocity logs that are measured in

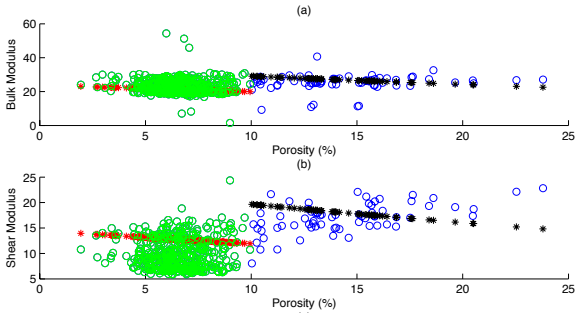


Figure 4: (a) A scatter plot of bulk modulus and porosity. (b) A scatter plot of shear modulus and porosity. In both plots, measurements in the shale sections (green circles) show lower porosity and lower modulus. Measurements in the sand sections (blue circles) show higher porosity and higher modulus. Red and black asterisks denote the HS upper bound for shale and sand, respectively.

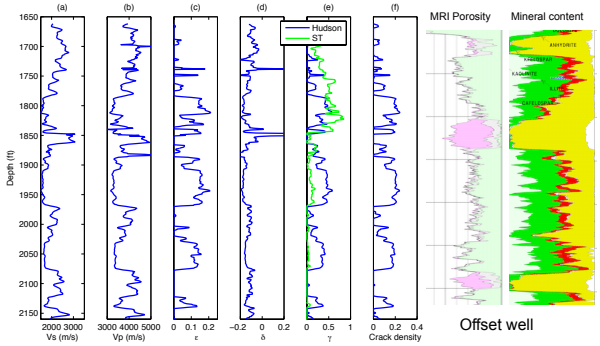


Figure 5: Elastic parameters measured and modeled by Hudson-Cheng's model. The MRIL$^{TM}$ porosity distinguishes the primary porosity (in purple) and the microporosity (in green). The mineralogy log denotes the relative content of quartz in yellow and illite in green. A comparison between the modeled $\gamma$ and the measured $\gamma$ from Stoneley waves shows that the Stoneley wave measurements are not reliable compared with the mineralogy logs from a nearby well.

(a) and (b), and the modeled anisotropy parameters $\varepsilon, \delta$ and $\gamma$ in (c), (d), and (e), respectively. In the sand layer, we estimated nearly no anisotropy. In the section above the sand layer around 1850 ft, the estimated $\gamma$ modeled using the crack model fits qualitatively with the $\gamma$ calculated from the Stoneley waves, although cannot be compared quantitatively. In the shale sections below the sand layer, Stoneley waves measure a much smaller shear wave anisotropy despite a similarity in mineralogy as shown in the offset well. On the other hand, anisotropy estimated from the proposed approach shows consistency with the illite content (in green) in the mineralogy log throughout the whole depth range. We have chosen a combination of $K_0$ and $\mu_0$ such that the anisotropy parameters $\varepsilon$ and $\delta$ fall in the expected range of shales. The $\delta$ value we estimated using the Hudson-Cheng's model are mostly negative, which might be the result of an excessive amount of illite (denoted in green in the mineralogy log) in the formation.

## DISCUSSIONS AND CONCLUSIONS

In this paper, we show that directional information about anisotropy can be derived from non-directional well logs and vertical measurements of the sonic wave velocities, based on the assumption of a crack model. Compared with previously proposed methods (Bandyopadhyay, 2009; Bachrach, 2010), the proposed method eliminates the need of estimating parameters that have little practical guidance. It presents a formalized workflow with less input parameters with clear physical meanings. Estimated anisotropy parameters can be used directly as initial solutions to seismic imaging and AVA inversion algorithms. Multiple realizations of the anisotropy parameters can also be used to construct the covariances among the elastic parameters (Li et al., 2016).

To obtain a consistent crack model, we solve a multi-parameter inverse problem by grid search. The objective function contains many local minima, especially with respect to the background shear modulus. Further constraints are applied to make sure the modeled anisotropy stays within the plausible ranges. However, this additional verification has to be performed after the inversion, which hinders the automation of the inversion and the model building process.

Challenges of accurately measuring $C_{66}$ by Stoneley waves are the main reason contributing to the mismatch between the shear anisotropy from the crack model and the shear anisotropy from Stoneley wave measurements. First of all, Stoneley wave is very sensitive to the borehole and the near borehole conditions. For example, a metal casing, despite its small thickness compared with the wavelength, will mask the response of the formation behind it. Similarly, any small change in the near borehole condition will change the Stoneley wave velocity significantly. Furthermore, even in a perfect borehole, Stoneley wave looses its sensitivity to SH waves in the fast formations (Cheng et al., 1983). Therefore, great caution should be practiced when estimating shear wave anisotropy from Stoneley wave measurements.

The anisotropy modeled using the proposed method might be overestimated due to the choice of Hashin-Shrikman background model, which attribute all the differences between the background and the estimated moduli to the aligned thin cracks. A softer background, comprised of both spherical and randomly distributed thin-cracks, would reduce the estimated anisotropy in the shale sections. To estimate the anisotropy due to organic matters in shale, a non-zero modulus should be used for the shear modulus of the pore fluid.

## ACKNOWLEDGEMENTS

The authors acknowledge the EDB Petroleum Engineering Professorship for their financial support and Halliburton for the well log data. Dr Yunyue Elita Li acknowledge the MOE Tier-1 Grant R-302-000-165-133 for financial support.

## REFERENCES


Bachrach, R., 2010, Applications of deterministic and stochastic rock physics modeling to anisotropic velocity model building: SEG Expanded Abstracts, **29**, 2436–2440.

Bandyopadhyay, K., 2009, Seismic anisotropy: geological causes and its implications: PhD thesis, Stanford University.

Cheng, C., 1993, Crack models for a transversely isotropic medium: Journal of Geophysical Research: Solid Earth, **98**, 675–684.

Cheng, C. H., M. N. Toksoz, et al., 1983, Determination of shear wave velocities in" slow" formations: Presented at the SPWLA 24th Annual Logging Symposium, Society of Petrophysicists and Well-Log Analysts.

Hashin, Z., and S. Shtrikman, 1962, A variational approach to the elastic behavior of multiphase materials: Journal of the Mechanical Physics of Solids, **11**, 127–140.

Hornby, B., L. M. Schwartz, and J. A. Hudson, 1994, Anisotropic effective-medium modeling of the elastic properties of shales: Geophysics, **59**, no. 10, 1570–1583.

Hudson, J. A., 1981, Wave speeds and attenuation of elastic waves in material containing cracks: Geophysical Journal International, **64**, 133–150.

Li, Y., B. Biondi, R. Clapp, and D. Nichols, 2016, Integrated VTI model building with seismic data, geologic information, and rock-physics modeling - Part 2: Field data test: Geophysics, **81**, C205–C218.

Li, Y., B. Biondi, D. Nichols, G. Mavko, and R. Clapp, 2013, Stochastic rock physics modeling for seismic anisotropy: SEP report, **149**, 201–220.

Li, Y., D. Nichols, K. Osypov, and R. Bachrach, 2011, Anisotropic tomography using rock physics contraints: $73^{rd}$ EAGE Conference & Exhibition.

Mavko, G., T. Mukerji, and J. Dvorkin, 2009, The rock physics handbook: Tools for seismic analysis of porous media: Cambridge university press.

Sayers, C., 1995, Anisotropic velocity analysis: Geophysical Prospecting, **43**, 541–568.

Tang, X., 2003, Determining formation shear-wave transverse isotropy from borehole Stoneley-wave measurements: Geophysics, **68**, 118–126.

Vernik, L., and X. Liu, 1997, Velocity anisotropy in shales: A petrophysical study: Geophysics, **62**, 521–532.

Yang, Y., K. Osypov, R. Bachrach, M. Woodward, O. Zdraveva, Y. Liu, A. Fournier, and Y. You, 2012, Anisotropic tomography and uncertainty analysis with rock physics constraints: Green Canyon case study: SEG Expanded Abstract, 1–5.